

# Differential-Fed Log-Periodic Dipole Array with High Isolation for Wideband Full-Duplex Communications

Tuan T. Nguyen\* and Tutku Karacolak

**Abstract**—This study presents a differentially driven log-periodic dipole array system with high isolation between reception and transmission ports for wideband full-duplex applications. The antenna system is composed of two pairs of log-periodic dipole arrays operating in the X-band spectrum from 8 GHz to 12 GHz. The system offers a low cross-polarization between  $E$ -plane and  $H$ -plane (less than  $-25$  dB). The simulation results show high isolation  $S_{21} < -60$  dB through the entire X-band while the measured results reach  $S_{21} < -45$  dB in a reflective lab room. Furthermore, in order to verify the measured values, a modified  $180^\circ$  out-of-phase wideband power divider is used to feed transmitting and receiving ports. The second measured outcomes also attain total isolation greater than 45 dB for the entire band of interest. The proposed design is able to cover both orthogonal transmitted and received directions with reasonable gain values, high efficiency, and good impedance matching.

## 1. INTRODUCTION

As the wireless communication devices are becoming more numerous, the available radio wave spectrum is becoming increasingly congested due to the traditional data transmission practices such as frequency- and time-division multiplexing. These methods require transmission (TX) and reception (RX) at either different frequencies or at different times, decreasing the spectral efficiency. Researchers are exploring new wireless spectrum standards to address overcrowded spectrum. One of these standards is full-duplex communications which allows for transmitting and receiving on the same frequency at the same time [1, 2]. In recent years, this technology has been broadly investigated and proved its significant role in various aspects of the technological advancements. Because the transmitted and received signals are reduced to a single frequency, more frequency resources are available for the data communication within a specified bandwidth leading to an efficient use of the RF spectrum. However, there are several challenges to realize full-duplex operation. The most significant of them is the high level of self-interference. The power of this undesired signal can be much stronger than the targeted signal [3]. Hence, the received signal of interest may become unrecognizable and distorted due to RF leakage between transmitting and receiving terminals.

To successfully suppress this self-interference, different active and passive suppression methods have been considered including antenna separation, placing absorbers between antenna elements, using circulators combined with analog cancellation tools, and antenna orientation [4–8]. The authors in [9–11] also considered dual polarization antennas structure to mitigate the self-interference. Another technique uses a near-field resonator or coupling element to enhance the isolation between antenna elements [12, 13]. However, these proposed architectures achieve high isolation only at the center frequency suffering from low bandwidth. They are also large in size and are not appropriate for low-cost compact systems.

---

Received 2 November 2020, Accepted 28 December 2020, Scheduled 5 January 2021

\* Corresponding author: Tuan Thanh Nguyen (tuan.nguyen3@wsu.edu).

The authors are with the School of Engineering and Computer Science, Washington State University, Vancouver, WA, USA.

In this study, we propose a differentially driven log-periodic dipole array (LPDA) system with large isolation between transmission and reception ports for wideband full-duplex communications. The antenna system consists of two pairs of LPDAs. High isolation and wide bandwidth are the important characteristics of the design. To maximize the isolation, orthogonal polarization is considered. The propagating directions of both transmitted and received signals are offset by  $90^\circ$  about the center of the system. The LPDAs in transmission and reception pairs are oriented in the opposite directions and on the same plane [14]. However, the directions of transmitted and received antennas are perpendicular to each other to ensure that both signals will not interfere with one another. Thus, the signals of the system can propagate in orthogonal directions for both operations and maximize the isolation.

Symmetry manipulation is also employed to attempt to reach a high level of isolation [15]. By attaching both antennas to a single module, a compact planar antenna system is designed. The antenna system is optimized to sustain a high level of isolation through the entire band of interest. The proposed design provides coverage for X-band spectrum which has common applications in radar, weather monitoring, or air traffic control.

## 2. ANTENNA DESIGN PROCESS

In this work, two antenna arrays are designed with each having two elements. LPDAs are chosen for antenna elements due to their broad bandwidth, low cross polarization, high gain, and highly directive patterns. FR4 is used for the substrate with a thickness  $h_1$  of 1.5 mm, a dielectric permittivity  $\epsilon_r$  of 4.4, and dielectric loss tangent  $\tan \delta$  of 0.02. For a desired directivity of 8 dB, the scale factor,  $\tau$ , and relative spacing,  $\sigma$ , are determined as 0.865 and 0.15, respectively. With these parameters, the number of dipoles,  $N = 8$ , and aperture angle,  $2\alpha = 25.36^\circ$ , are calculated. Then, the length of the largest dipole is computed using the lowest frequency of operation.

Considering the  $50 \Omega$  characteristic impedance,  $Z_n$ , the width,  $W_n$ , is found using the below expressions [16]:

$$Z_n = \frac{\eta_0}{\pi} \left[ \ln \left( \frac{L_n}{a_n} \right) - 2.25 \right] \quad (1)$$

$$W_n = \pi a_n \quad (2)$$

where  $a_n$  is the radius of each cylindrical dipole, and  $\eta_0$  is the intrinsic impedance of air.

Finally, after computing the dimensions of the largest dipole, the length,  $L$ , width,  $W$ , and spacing,  $D$ , of remaining dipoles are determined by using the following well-known LPDA design expressions:

$$\frac{1}{\tau} = \frac{L_{n+1}}{L_n} = \frac{W_{n+1}}{W_n} = \frac{D_{n+1}}{D_n} \quad (3)$$

Figure 1(a) illustrates the geometry of a single LPDA antenna. The optimized dimensions of the LPDA are given in Table 1. The mode converter balun based on tapered microstrip lines is used for impedance matching and feeding the LPDA. Figure 1(b) depicts the top view of proposed LPDA antenna

**Table 1.** Geometry of the proposed LPDA.

Dipole	Length, $L_n$ (mm)	Width, $W_n$ (mm)	Spacing, $D_n$ (mm)
1	2.391	0.688	
2	2.764	0.795	2.081
3	3.196	0.920	2.406
4	3.694	1.063	2.782
5	4.271	1.229	3.216
6	4.938	1.421	3.718
7	5.709	1.643	4.299
8	6.600	1.900	4.970

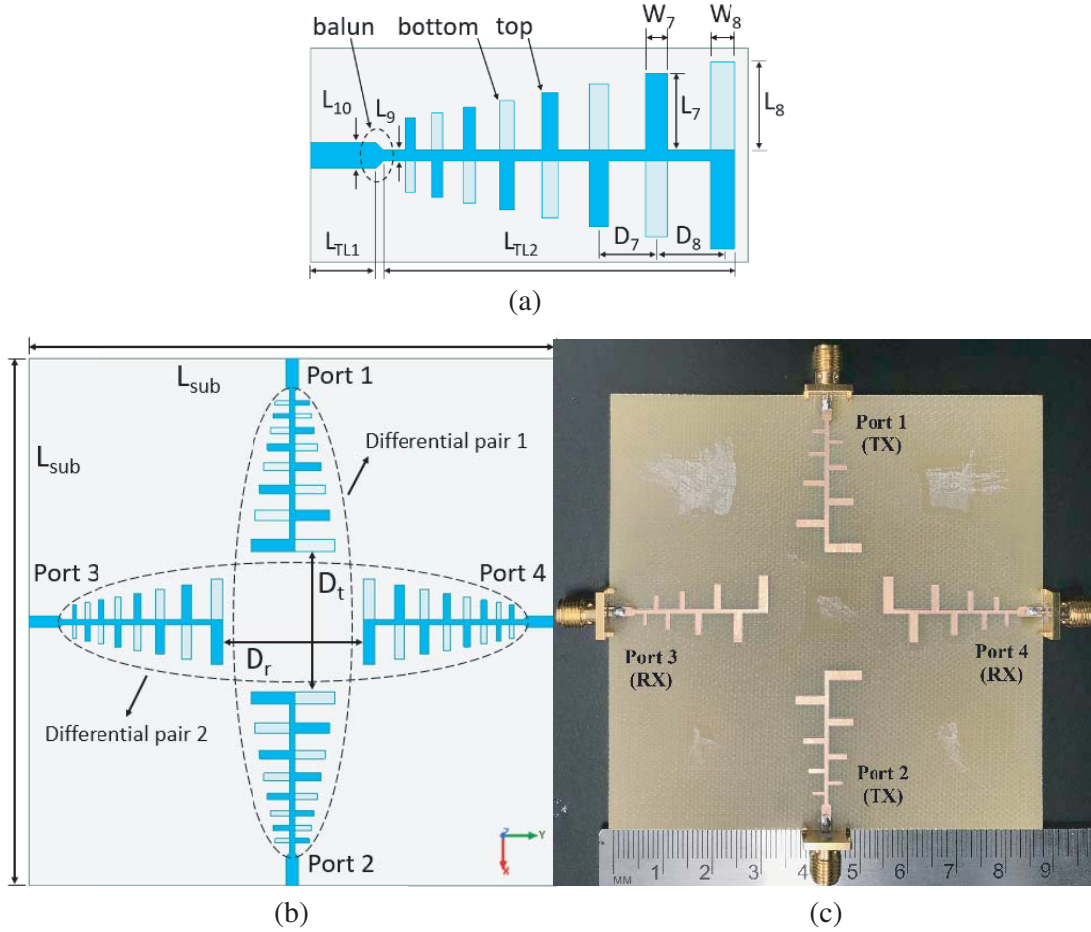


**Figure 1.** (a) The geometry of a single LPDA; (b) The geometry of LPDA antenna system; (c) The top view of the fabricated system.

system with two differential pairs. Here, we assign ports 1 and 2 as differential port 1 (TX port), and ports 3 and 4 as differential port 2 (RX port). This design provides orthogonal linear polarizations in the same radiating structure. Dual linear polarizations in the horizontal and vertical planes will effectively suppress the coupling between the two differential pairs without affecting antenna’s radiation performance. The TX and RX LPDAs are separated by an optimized distance  $D_t$  and  $D_r$  of  $0.928\lambda$ , where  $\lambda$  is the wavelength of the highest frequency. The spacing between two opposite LPDAs is important since it affects the mutual coupling and beam direction of the array between TX and RX ports. Figure 1(c) shows the fabricated antenna system which comprises four LPDAs. The bottom side of each LPDA is symmetrical with the top side and is soldered to the ground part of the SMA connector.

The reflection coefficients and isolation for the antenna system are calculated using two methods. In the first method, the differential pair 1, which includes the single-ended ports 1 and 2, is designated as differential TX port 1. Likewise, the differential pair 2 including ports 3 and 4 is designated as differential RX port 2. The differential simulated and measured  $S$ -parameters are obtained using the below equations [17]:

$$S_{a11} = \frac{1}{2} (S_{11} - S_{12} - S_{21} + S_{22}) \tag{4}$$

$$S_{a22} = \frac{1}{2} (S_{33} - S_{34} - S_{43} + S_{44}) \tag{5}$$

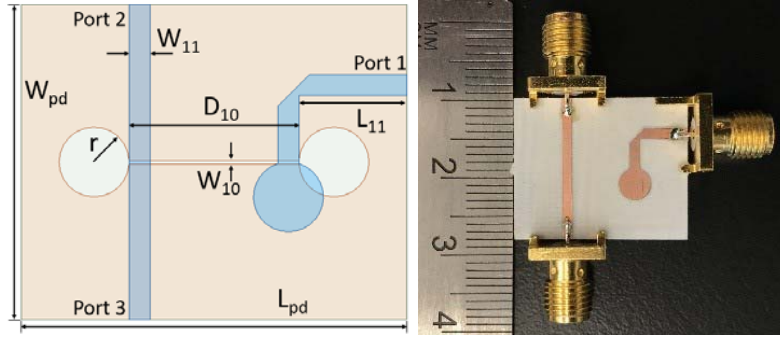


**Figure 2.** The top-view of the wideband power divider.

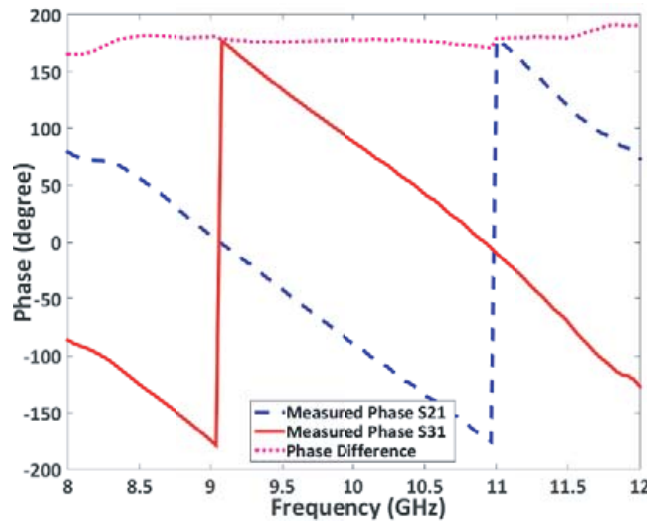


**Figure 3.** Measured phase of output ports for the modified power divider.

$$S_{a12} = \frac{1}{2} (S_{13} - S_{14} - S_{23} + S_{24}) \quad (6)$$

$$S_{a21} = \frac{1}{2} (S_{31} - S_{41} - S_{32} + S_{42}) \quad (7)$$

where  $S_{ij}$  are single-ended S-parameters for an ordinary 4-port device. Here,  $S_{a11}$  and  $S_{a22}$  denote the differential reflection coefficients, and  $S_{a12}$  and  $S_{a21}$  show the coupling between differential TX and RX ports. Moreover, to further validate the results, two wideband  $180^\circ$  out-of-phase power dividers are implemented based on the design in [18] to feed each differential pair. Because two LPDAs in each pair are placed opposite to each other,  $180^\circ$  power divider is chosen for feeding method. Note that the design in [18] operates from 3 GHz to 10 GHz, and we redesigned the original model to cover the entire X-band spectrum. Power divider is designed on a RO4003C substrate with dielectric permittivity  $\epsilon_r$  of 3.66, thickness  $h_2$  of 0.51 mm (0.020 in), and loss tangent  $\tan \delta$  of 0.0031. The geometry of the power divider is shown in Figure 2. It achieves phase difference of  $180^\circ$  between the output ports through the operating band, as seen in Figure 3. Table 2 shows the detailed dimensions of the entire antenna system.

### 3. RESULTS AND DISCUSSION

The antenna system is designed and simulated by using ANSYS HFSS. Based on the first method, the differential reflection coefficients ( $S_{a11}$  and  $S_{a22}$ ) and the isolation of differential signal between TX and

**Table 2.** Geometry of the proposed antenna system.

Symbol	Dimension (mm)	Symbol	Dimension (mm)
$L_{TL1}$	4.85	$L_{pd}$	22.0
$L_{TL2}$	26.4	$W_{pd}$	18.0
$D_r$	23.2	$W_{10}$	0.20
$D_t$	23.2	$D_{10}$	9.70
$L_9$	0.80	$W_{11}$	0.90
$L_{10}$	1.90	$L_{11}$	6.15
$L_{sub}$	87.8	$r$	2.00

RX ports ( $S_{a21}$ ) are calculated using Eqs. (4)–(7). An Agilent PNA-L Network Analyzer N5230C is used to measure the  $S$ -parameters in a reflective environment. The LPDA operates from 6 GHz to 12 GHz; however, we only focus on X-band spectrum with large isolation. Figure 4 illustrates the simulated and measured results of the proposed system. The simulated reflection coefficients show that both TX and RX antennas operate through the entire X-band spectrum. The measured impedance matching is good from 8 GHz to 11.4 GHz and degraded in the higher frequencies after 11.4 GHz.

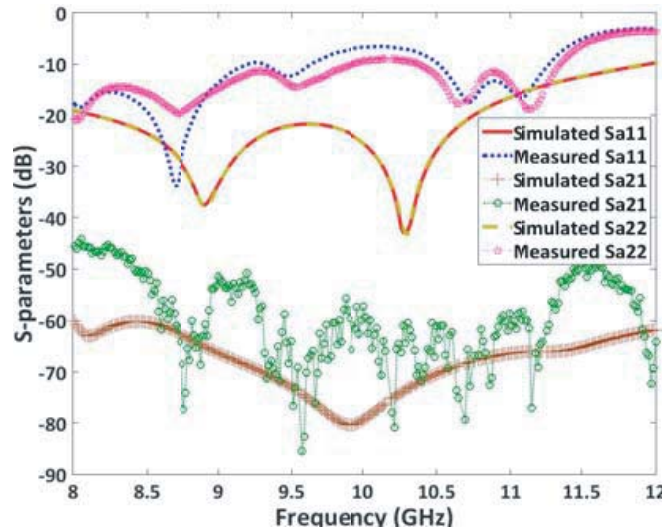


**Figure 4.** Simulated and measured  $S$ -parameters using first method.

Additionally, the system maintains high simulated isolation,  $S_{a21} < -60$  dB, attaining  $-80$  dB at the center of the band. The measured results indicate that the system sustains high isolation  $S_{a21} < -45$  dB, reaching as low as  $-85$  dB. The difference between the simulated and measured data may be caused by several factors. The losses of the SMA connectors affect the antenna matching. The imperfections account for the fabrication process of the mini milling machine. Also, regarding the isolation, reflections from the environment and symmetricity degradation due to the coaxial cables limit the amount of isolation that can be measured.

As previously mentioned, further measurements have been performed with the use of two out-of-phase power dividers. As shown in Figure 5, each differential LPDA pair is connected with a wideband power divider using coaxial cables. Figure 6 clearly illustrates that the system maintains a high isolation less than  $-45$  dB and reaches a minimum of  $-78$  dB. The antenna also has good impedance matching, leading to a  $-10$  dB bandwidth from 8 GHz to 11.4 GHz within X-band. The second measurement method is in decent agreement with a bandwidth of 3400 MHz (35%), compared to the first method.

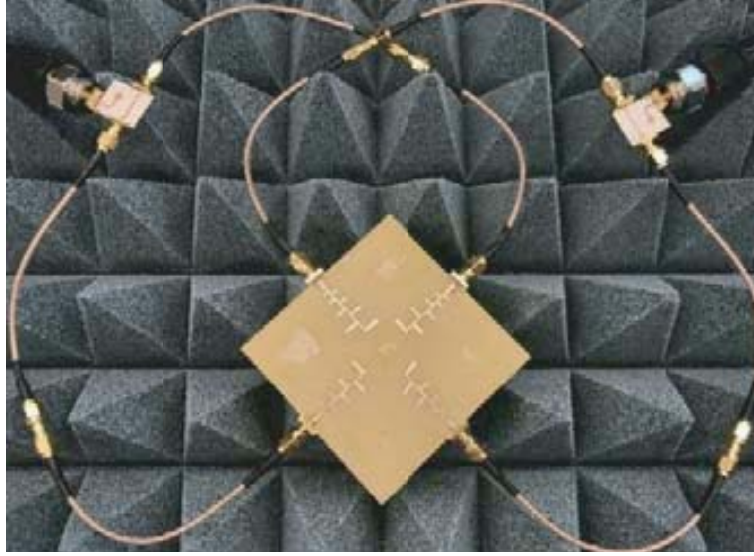


**Figure 5.** Measurement setup of the antenna system with wideband power dividers.

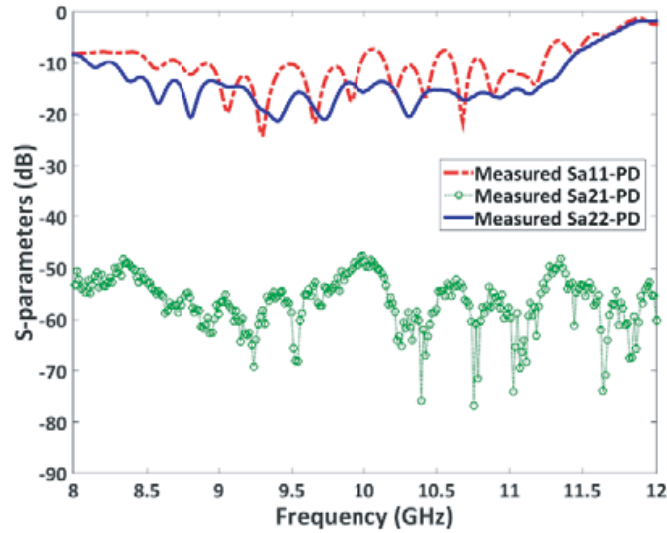


**Figure 6.** Measured  $S$ -parameters with power divider.

In Figure 7, the LPDA reaches simulated peak gain from 6.1 dB to 7.5 dB while the measured gain attains up to 7 dB. In order to measure the antenna gain, the coupling between two identical antennas is collected. Two LPDAs are placed line of sight and separated with a far-field distance  $2D^2/\lambda$ , where  $D$  is the maximum dimension of the LPDA, and  $\lambda$  is the wavelength of the highest frequency. Then, Friis transmission equation is used to calculate the gain in far-field region [19]:

$$\frac{P_r}{P_t} = |S_{21}|^2 = G_t G_r \left( \frac{\lambda}{4\pi R} \right)^2$$

where the ratio of the received to the input power,  $\frac{P_r}{P_t}$ , equals the transmission coefficient  $|S_{21}|^2$  measured by network analyzer. Since  $G_t$  and  $G_r$  are the gains of two identical antennas,  $G_t$  is equal to  $G_r$ . The distance between two antennas,  $R$ , is equal to or greater than the far-field distance. The scatterings and reflections from the environment cause the difference between the simulated and measured gains.

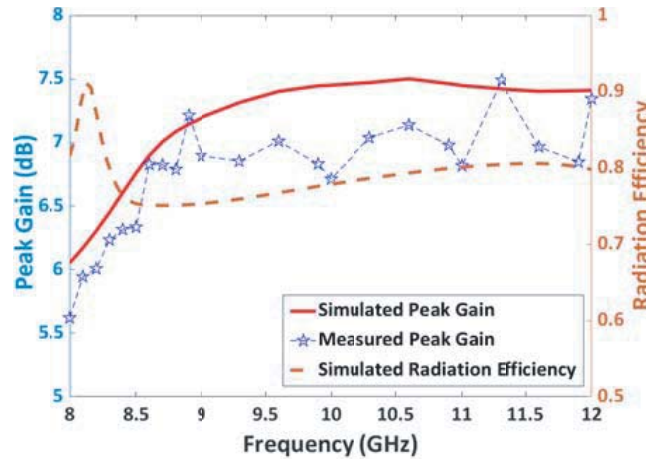


Figure 7. Simulated and measured gain of the antenna system.

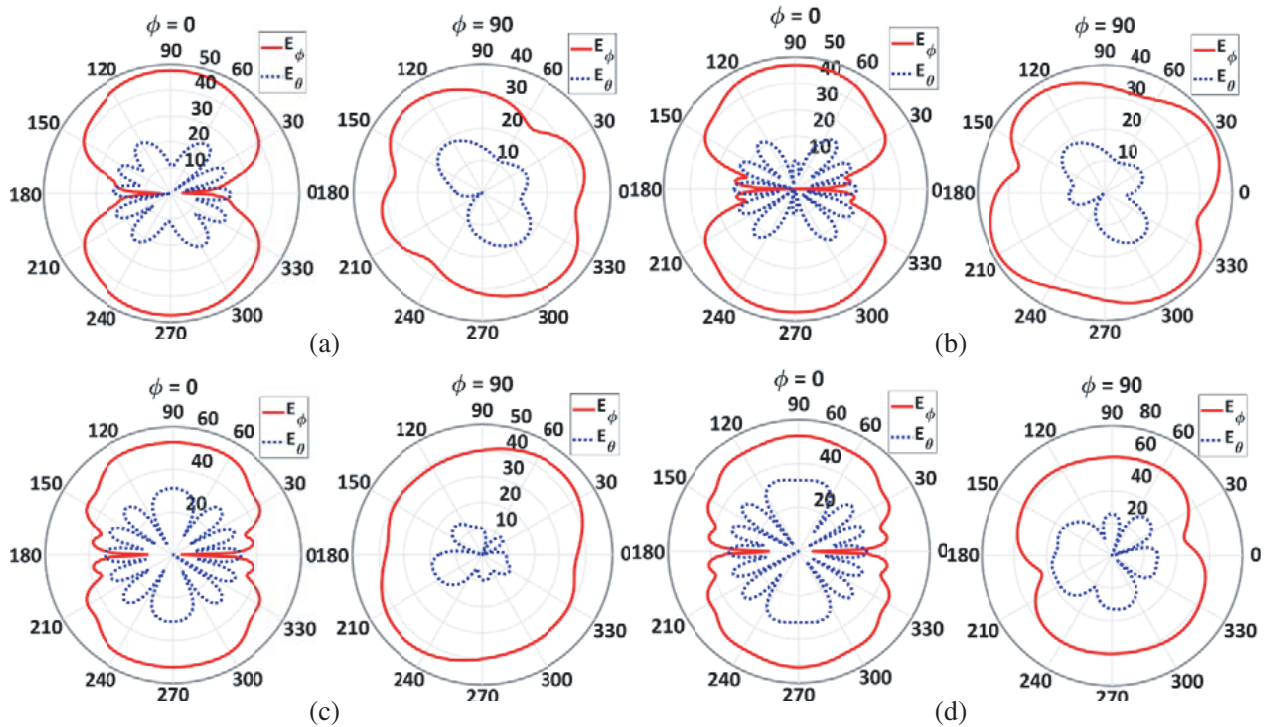
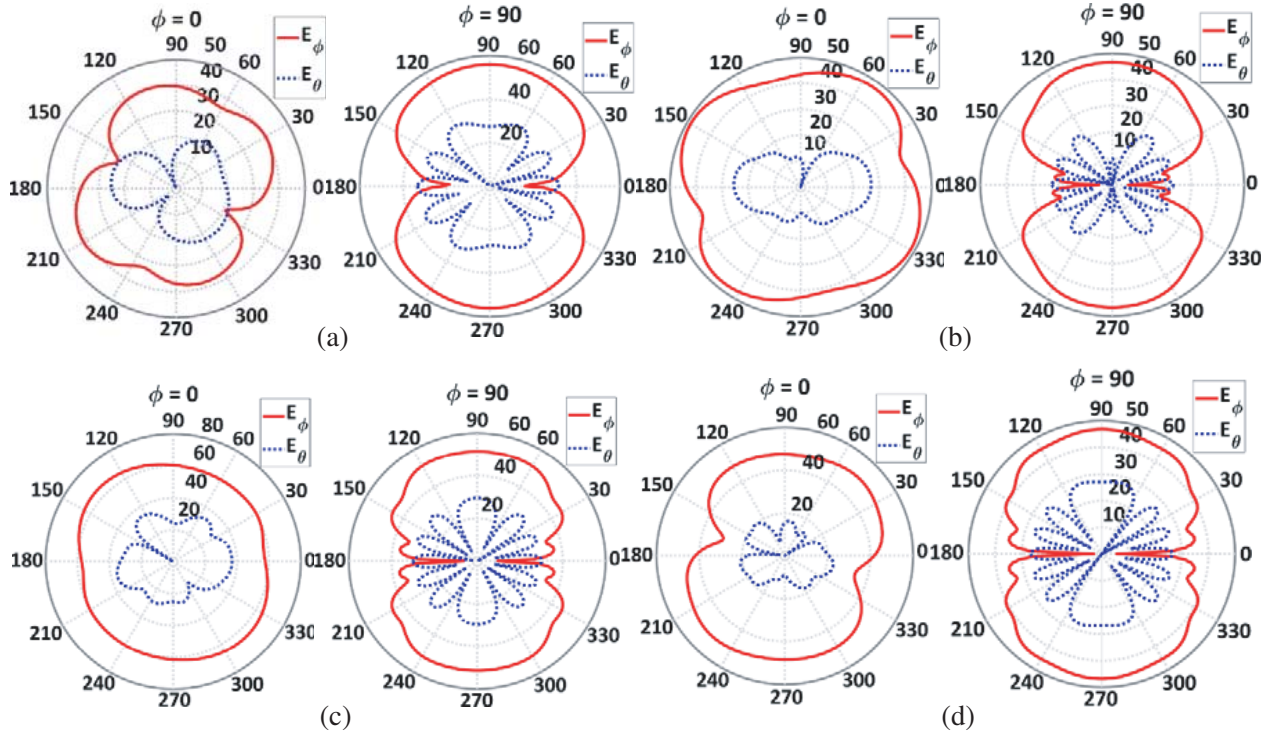


Figure 8. Radiation pattern of transmit mode with  $\Phi = 0^\circ$  and  $\Phi = 90^\circ$  at (a) 8 GHz, (b) 9 GHz, (c) 10 GHz, (d) 11 GHz.

Figure 7 also shows the simulated radiation efficiency of the antenna system sustaining more than 75% through the entire X-band which is good for radar applications. Figures 8 and 9 report the simulated co-polarized and cross-polarized radiation patterns of TX and RX modes at 8, 9, 10, and 11 GHz, respectively. In TX mode, the polarization differences approximate 39 dB and 21 dB at  $\phi = 0^\circ$  and  $\phi = 90^\circ$ , respectively. At  $\phi = 0^\circ$  ( $x$ - $z$  plane), the co-polarization value of RX mode is 25 dB more than cross-polarization value, while this value increases up to 38 dB in the directions of  $90^\circ$  and  $270^\circ$  at  $\phi = 90^\circ$  ( $y$ - $z$  plane). Additionally, the radiation patterns in  $E$ -plane are nearly omnidirectional, whereas they are almost bi-directional in  $H$ -plane over the operating frequency band. In TX mode, these values are similar due to symmetrical geometry of the antenna. Low cross-polarization prevents the interference between two signals and improves the performance of the system.



**Figure 9.** Radiation pattern of receive mode with  $\Phi = 0^\circ$  and  $\Phi = 90^\circ$  at (a) 8 GHz, (b) 9 GHz, (c) 10 GHz, (d) 11 GHz.

**Table 3.** Comparison of the proposed system with literature.

Design	Targeted Frequency (GHz)	Measured Minimum Isolation (dB)	Bandwidth (%)
[1]	6	$< -55$	8.3
[4]	2.4	$< -46$	1
[9]	2.4	$< -50$	3.7
[10]	2.4	$< -40$	12.5
[20]	2.4	$< -50$	12.5
This work	X-band	$< -45$	35

Table 3 presents the comparison of the proposed antenna with high isolation full-duplex systems from the literature. As seen, the current design achieves a higher cancellation within a wide-band operation. The antenna array also maintains a high gain and low cross-polarization in a compact size.

#### 4. CONCLUSION

This paper presents a wideband high isolation antenna system for X-band full-duplex applications. The proposed design has two differentially-fed LPDA pairs for RX and TX operations. The structure maintains isolation greater than 45 dB through the entire band of interest in a highly reflective environment. A stable radiation pattern with low cross-polarization values is observed and covers orthogonal directions for both RX and TX modes. This compact antenna system with its high isolation and gain can be used within small size wideband full-duplex systems.

## REFERENCES

1. Douglas, T. J. and K. Sarabandi, "A High-Isolation Two-Port Planar Antenna System for Communication and Radar Applications," *IEEE Access*, Vol. 6, 9951-9959, 2018.
2. Sabharwal, A. *et al.*, "In-Band Full-Duplex Wireless: Challenges and Opportunities", *IEEE J. Sel. Areas Commun.*, Vol. 32, No. 9, 1637-1652, 2014.
3. Wang, X., W. Che, W. Yang, W. Feng, and L. Gu, "Self-Interference Cancellation Antenna Using Auxiliary Port Reflection for Full-Duplex Application," *IEEE Antennas and Wireless Propagation Letters*, Vol. 16, 2873-2876, 2017.
4. Everett, E., A. Sahai, and A. Sabharwal, "Passive Self-Interference Suppression for Full-Duplex Infrastructure Nodes," *IEEE Trans. on Wireless Comm.*, Vol. 13, No. 2, 680-694, 2014.
5. Bharadia, D., E. McMillin, and S. Katti, "Full Duplex Radios," *ACM SIGCOMM Comput. Commun. Rev.*, Vol. 43, No. 4, 375-386, 2013.
6. Hong, S., J. Mehlman and S. Katti, "Picasso: Flexible RF and spectrum slicing," in *Proc. 2012 SIGCOMM*, 1-5.
7. Etellisi, E. A., M. A. Elmansouri, and D. S. Filipovic, "Wideband monostatic simultaneous transmit and receive (STAR) antenna," *IEEE Trans. Antennas Propag.*, Vol. 64, No. 1, 6-15, 2016.
8. Zhang, Z., X. Chai, K. Long, A. V. Vasilakos, and L. Hanzo, "Full duplex techniques for 5G networks: self-interference cancellation, protocol design, and relay selection," *IEEE Communications Magazine*, Vol. 53, No. 5, 128-137, 2015.
9. Goodbody, C., T. Karacolak, and N. Tran, "Dual-polarised patch antenna for in-band full-duplex applications," *Electronics Letters*, Vol. 54, No. 22, 1255-1256, 2018.
10. Sim, C. Y. D., C. C. Chang, and J. S. Row, "Dual-feed dual-polarized patch antenna with low cross polarization and high isolation", *IEEE Trans. Antennas Propag.*, Vol. 57, No. 10, 3405-3409, 2009.
11. Zarifeh, N., M. Alissa, M. Khaliel, and T. Kaiser, "Self-interference mitigation in full-duplex base-station using dual polarized reflect-array," in *2018 11th German Microwave Conference (GeMiC)*, Freiburg, 180-183.
12. Li, M., B. G. Zhong, and S. W. Cheung, "Isolation Enhancement for MIMO Patch Antennas Using Near-Field Resonators as Coupling-Mode Transducers," *IEEE Transactions on Antennas and Propagation*, Vol. 67, No. 2, 755-764, 2019.
13. Hwang, J. and S. Chung, "Isolation Enhancement Between Two Packed Antennas With Coupling Element," *IEEE Antennas and Wireless Propagation Letters*, Vol. 10, 1263-1266, 2011.
14. Laco, J. M., F. H. Gregorio, G. Gonzalez, and J. E. Cousseau, "Patch Antenna Design for Full-Duplex Transceivers," in *2017 European Conf. on Networks and Communications (EuCNC)*, Oulu, Finland, 1-5.
15. Makar, G., D. Kim, N. Tran, and T. Karacolak, "Compact Antennas with Reduced Self Interference for Simultaneous Transmit and Receive," *Progress in Electromagnetics Research C*, Vol. 78, 19-31, 2017.
16. Carrel, R., "Analysis and design of the log-periodic dipole antenna," Ph.D. dissertation, Univ. of Illinois, Champaign, IL, USA, 1961.
17. Xue, Q., S. W. Liao, and H. X. Jian, "A differentially-driven dual-polarized magneto-electric dipole antenna," *IEEE Trans. Antennas Propag.*, Vol. 61, No. 1, 425-430, 2013.
18. Bialkowski, M. E. and A. M. Abbosh, "Design of a compact UWB out-of-phase power divider," *IEEE Microw. Wireless Compon. Lett.*, Vol. 17, No. 4, 289-291, 2007.
19. Hasan, Md. R., M. A. Riheen, P. Sekhar, and T. Karacolak, "Compact CPW-fed circular patch flexible antenna for super-wideband applications," *IET Microw. Antennas Propag.*, Vol. 14, No. 10, 1069-1073, 2020.
20. Goodbody, C., N. Tran, and T. Karacolak, "Patch Antenna for Full Duplex Application with Improved Isolation Using Defected Ground Structure," *Progress in Electromagnetics Research Letters*, Vol. 84, 91-97, 2019.